Structural Engineering and Mechanics, *Vol. 71, No. 1 (2019) 23-35*
DOI: https://doi.org/10.12989/sem.2019.71.1.023

Electro-elastic analysis of functionally graded piezoelectric variable thickness rotating disk under thermal environment

Mohammad Arefi* and Sina Kiani Moghaddam[a]

Faculty of Mechanical Engineering, Department of Solid Mechanics, University of Kashan, Kashan 87317-51167, Iran

(Received October 9, 2018, Revised December 3, 2018, Accepted December 5, 2018)

Abstract. In this study we derive the governing equations of a functionally graded piezoelectric disk, subjected to thermo-electro-mechanical loads. First order shear deformation theory is used for description of displacement field. Principles of minimum potential energy is used to derive governing equations in terms of components of the displacement field and the electric potential. The governing equations are derived for a disk with variable thickness. The numerical results are presented in terms of important parameters of the problem such as profile of variable thickness, in-homogeneous index and other related parameters.

Keywords: electro-elastic; functionally graded piezoelectric disk; variable thickness; first order shear deformation theory

1. Introduction

Functionally graded materials (FGMs) are defined as those materials in which the volume fraction of the two or more materials is varied as a power-law distribution. This distribution varies continuously as a function of position along with certain dimensions of the structure from one point to another (Reddy 2000, Suresh and Mortensen 1998). Usually, a ceramic is used at one surface to resist severe environmental effects such as temperature, corrosion and wear (Afsar and Go 2010). The original purpose of functionally graded materials was to develop thermal barrier coatings for propulsion systems of spacecraft to resist high temperature and to ensure high thermal conductivity as well (Holt *et al*. 1993). Rotating disks have extensive practical engineering applications, such as, in steam and gas turbines, turbo generators, flywheel of internal combustion engines, turbojet engines, etc. Brake disks and clutch are examples of solid rotating disks where body forces and bending loads are applied. Gas turbine rotor can be assumed as a clamped-free condition by ignoring thermal expansion. In all of these applications, the performance of the components in terms of efficiency, service life and power transmission, certainly depend on the material, speed of rotation and operating conditions. However, for special application such as aerospace, where lightweight and durability becomes crucial in high temperatures, the components need to be fabricated using FGM materials (Bayat *et al*. 2009).

Reddy, Wang and Kitipornchai (1999) have studied axisymmetric bending and stretching of FG solid and annular circular plates using First Order Shear Deformation Theory (FSDT). The solutions for deflection, force and moment resultants were presented in terms of the corresponding quantities of isotropic plates based on the classical Kirchhoff plate theory. Parveen and Reddy (1998) have used the FSDT and derived the equilibrium and stability equations of a moderately thick rectangular plate made of FGM under thermal loads. They assumed that the material properties varied as a power law of thickness. Bayat (2007) have developed a new set of equilibrium equations with small and large deflections in a FG rotating disk with axisymmetric bending and steady state thermal loadings. The material properties of the disk varied in the thickness direction. FSDT and von Karman theories were used in this study. Li, Ding and Chen, 2006 have obtained an elastic solution for pure bending problems of simply supported, transversely isotropic circular plates with elastic compliance coefficient being arbitrary functions of the thickness coordinates. Chen (2007) have obtained a three-dimensional analytical solution for transversely isotropic FG rotating plate by means of the direct displacement method. The displacement components were assumed as a linear combination of certain explicit functions of the radial coordinates. Li, Ding and Chen (2008) have used the stress function method and presented a set of elasticity solutions for the axisymmetric problem of transversely isotropic, simply supported and clamped edge FG circular plates subjected to a transverse load. They illustrated the effect of material in-homogeneity on the elastic field in FG plates.

In the study conducted by Durodola and Attia (2000), a finite element analysis is adopted for FG rotating disks using a commercial software package. The disks were modeled as non-homogeneous orthotropic materials such as those obtained through non-uniform reinforcement of metal matrix by long fibers. They considered three types of

*Corresponding author, Assistant Professor
E-mail: arefi@kashanu.ac.ir
[a] M.Sc. Student
E-mail: sinakiani@grad.kashanu.ac.ir

http://www.techno-press.com/journals/sem&subpage=7
ISSN: 1225-4568 (Print), 1598-6217 (Online)

gradation distribution for the Young's modulus in the hoop direction relative to the matrix modulus. Jahed and Sherkatti (2000) have applied the Variable Material Properties method (VMP) and obtained stresses for an in-homogeneous rotating disk with variable thickness under steady temperature field, assuming the material properties as the field values. Kheirkhah and Loghman (2015) studied the stress and electric potential redistribution of thick walled FGP cylinder due to creep using a semi analytical method. Dai and Dai (2017) investigated thermal loadings on a variable thickness FGMME material with radial polarization. They have obtained electric and magnetic potentials as well as stresses and displacements with different grading parameters by a semi-analytical solution.

Arefi and Rahimi (2012) have presented a non-linear analysis of a FGP annular plate, based on Von-Karman assumptions. The response of a system can be obtained using minimization of the energy of system with respect to amplitude of displacements and electric potential. In a study conducted by Arefi and Zenkour (2017b), Thermo-electro-mechanical bending behaviour of sandwich nano-plate integrated with piezoelectric face sheets based on trigonemtric plate theory used the trigonometric shear and normal deformation plate theory to study the thermo-electro-mechanical bending analysis of a sandwich nano plate.

There are also other efficient computational methods for solving electro-elastic problems that can solve wider range of problems that are currently the key topic under study by many researchers. Nanthakumar, Lahmer, Zhuang, Zi and Rabczuk (2016) have proposed an algorithm to solve the inverse problem of identifying piezoelectric material interfaces.

Iterative extended finite element formulation was used in their analysis. They claim that the algorithm offered can provide a smart way of health monitoring piezoelectric or flexoelectric structures. The method was also optimized to apply for broad ranges of problems (Hamdia *et al*. 2017). Thai, Rabczuk and Zhuang (2018) have provided an isogeometric approach to analyze large deformation of electro-mechanical problems by applying non-uniform rational B-spline function. Numerical solutions for various problems of flexoelectric effects prove the efficiency of this method especially for soft materials. Hamdia *et al*. (2017) have presented a sensitivity analysis to identify the key parameters affecting the energy conversion factor. IGA was first applied to formulate the problem and the various methods such as MOAT and EFAST were involved in the sensitivity analysis. Nguyen, Zhuang and Rabczuk (2018) have used a numerical model for the characterization of Maxwell-Wagner relaxation in piezoelectric and flexoelectric composite material where they presented a numerical model of the Maxwell-Wagner polarization effect in a piezoelectric bi-layer structure. Furthermore, effective dielectric permittivity, piezoelectric coefficient and flexoelectric coefficients as well as their frequency dependence were investigated in this study. Nguyen, et al., 2018 studied the dynamic flexoelectric effects and natural frequencies on a simply supported beam. The numerical results reveal the importance of the dynamic flexoelectric coefficient. Various methods for quantifying uncertain parameters are also available (Hamdia *et al*. 2017). Vu Bac *et al*. (2016) provided a sensitivity analysis toolbox using MATLAB functions that help quantifying the effect of various parameters for an output goal.

A comprehensive investigation on the elastic, thermo-elastic and electro-elastic analysis of disks and plates was performed. The literature review of this study indicates that although some useful research pieces on the electro-elastic analysis of functionally graded disk were conducted, however, the absence of a comprehensive work on the electro-elastic analysis of functionally graded radially polarized variable thickness rotating disk is noticeable in the literature. Moreover, a research is needed to investigate the possible application of variable thickness FGPM rotating disk to be used as a turbine disk to produce electricity. In this study, we employ first order shear deformation theory to present thermo-electro-elastic analysis of functionally graded variable thickness disk subjected to thermal, mechanical and electrical loads. These loads are presented in the form of rotational body force, radial temperature distribution and applied electric charges. Furthermore, the boundary conditions are assumed to be clamped-free at the inner and outer sides of the disk. The influence of important parameters such as type of profile, electric loads, gradation of material properties and dimensionless geometric parameters have been taken into account.

2. Gradation of material properties

In this research, electro-elastic results of a functionally graded piezoelectric disk with variable thickness are studied. All of the mechanical, electrical and thermal material properties are assumed to be variable along the thickness direction, based on power-law distribution. For a symbolic material properties $P(z)$, the following relations are expressed as (Arefi and Allam 2015, Arefi 2015, Arefi *et al*. 2011, Arefi and Rahimi 2011)

$$P(z) = (P_u - P_l) \cdot \left(\frac{z - z_l}{z_u - z_l}\right)^n + P_l \tag{1}$$

Where; $P(z)$ denotes the material property P_u and P_l denote the property of the upper and lower surface properties respectively. n is known as the grading index (Zenkour and Mashat 2011, Arefi and Rahimi 2011). In this study the two types of materials used are both PZT ceramics, with PZT5 ceramic at the lower surface and PZT4 at the top surface. Both the density (ρ) and thermal conductivity (k) are the same values for both materials and hence, there is no variation for these parameters along the thickness direction.

A schematic of the variable disk can be observed in Fig. 1.

3. Temperature distribution

In this study, a distributed temperature field in the radial coordinate has been taken into account by neglecting the

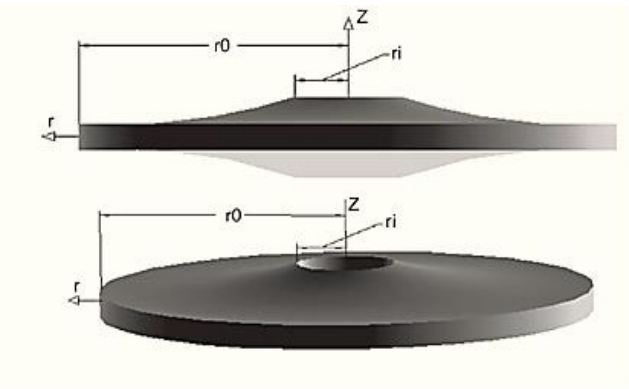

Fig. 1 Schematic of a variable thickness disk

thermal changes through the thickness, which is presented by the steady state heat conduction equation. The heat transfer equation is expressed as (Arefi and Rahimi 2014):

$$\frac{1}{r}\left(rkT'(r)\right)' = 0 \tag{2}$$

The boundary conditions regarding Eq. (2) are:

$$T(r_i) = T_i \ , T(r_o) = T_o \tag{3}$$

Where; r_i and r_o represent the inner and outer radius of the disk. The solution of the Eq. (2) and the corresponding boundary conditions result in:

$$T(r) = \frac{T_o - T_i}{ln(^{r_o}/_{r_i})} ln(r) + \frac{T_i ln(r_o) - T_o ln(r_i)}{ln(^{r_o}/_{r_i})} \tag{4}$$

4. Electro-elastic formulation of variable thickness disk

A variable thickness annular FGP disk is considered in this paper. The profile thickness is expressed as a power function (Zenkour and Mashat 2011, Arani *et al*. 2010). The thickness profile is described as:

$$h(r) = h_0[1 - q\left(\frac{r}{r_0}\right)^m] \tag{5}$$

Where; h_0 is the thickness at the axis of the disk. q and m are geometric parameters with the condition of $0 \le q \le 1$ and $m \ge 0$. A uniform thickness is obtained by setting $q = 0$ and a linearly decreasing thickness is obtained by setting $m = 1$. For $m > 1$ and $m < 1$ equation would result in a convex and concave profile respectively.

The first order shear deformation Theory (FSDT) is the most straight forward theory that accounts for non-zero transverse shear strain. Based on FSDT, the displacement field is described as:

$$u_r = u_0(r) + z\psi(r) \ , \ u_\theta = 0 \ , \ u_z = w(r) \tag{6}$$

Where; u_r, u_θ and u_z are the radial, circumferential and axial displacements respectively. $u_0(r)$ is known as the in-plane displacement of the middle surface of the disk. ψ denotes the rotation of a transverse normal in θ plane and $w(r)$ is displacement in the thickness direction. Since the problem is axisymmetric u_θ is zero. The strain-displacement relations are given by:

$$\begin{gathered}\varepsilon_r = \frac{\partial u_r}{\partial r} = u'(r) + z\psi'(r) \\ \varepsilon_\theta = \frac{u_r}{r} = \frac{u(r)}{r} + \frac{z\psi(r)}{r} \\ \gamma_{rz} = 2\varepsilon_{rz} = \frac{\partial u_r}{\partial z} + \frac{\partial u_z}{\partial r} = \psi(r) + w'(r) \\ \gamma_{r\theta} = \gamma_{\theta z} = \varepsilon_z = 0\end{gathered} \tag{7}$$

Throughout this study, prime denotes the derivative with respect to the radial coordinates. The stress-strain relations considering thermal strains and electric effects are expressed as three-dimensional multi-field equations of a functionally graded piezoelectric thick shell with variable thickness, curvature and arbitrary nonhomogeneity (Deneva *et al*. 2014, Arefi and Rahimi 2012).

$$\begin{gathered}\begin{Bmatrix}\sigma_{rr}\\ \sigma_{\theta\theta}\\ \sigma_{zz}\\ \sigma_{\theta z}\\ \sigma_{rz}\\ \sigma_{r\theta}\end{Bmatrix} = \begin{bmatrix} C_{11} & C_{12} & C_{13} & 0 & 0 & 0\\ C_{12} & C_{11} & C_{13} & 0 & 0 & 0\\ C_{13} & C_{13} & C_{33} & 0 & 0 & 0\\ 0 & 0 & 0 & C_{55} & 0 & 0\\ 0 & 0 & 0 & 0 & C_{55} & 0\\ 0 & 0 & 0 & 0 & 0 & \frac{C_{11}-C_{12}}{2}\end{bmatrix} \\ \begin{Bmatrix}\varepsilon_{rr} - \alpha_1 T\\ \varepsilon_{\theta\theta} - \alpha_1 T\\ \varepsilon_{zz} - \alpha_3 T\\ \gamma_{\theta z}\\ \gamma_{rz}\\ \gamma_{r\theta}\end{Bmatrix} - \begin{bmatrix} 0 & 0 & e_{31}\\ 0 & 0 & e_{31}\\ 0 & 0 & e_{33}\\ 0 & e_{15} & 0\\ e_{15} & 0 & 0\\ 0 & 0 & 0\end{bmatrix}\begin{Bmatrix}E_r\\ E_\theta\\ E_z\end{Bmatrix}\end{gathered} \tag{8}$$

In which; C_{ij} represent the stiffness coefficients, e_{ij} piezoelectric coefficients, α_i thermal expansions and E_i electric field components. The above parameters are assumed to be independent of the temperature for the chosen thermal environment. The electric displacement components along the radial, circumferential and transverse directions are expressed as:

$$\begin{gathered}\begin{Bmatrix}D_r\\ D_\theta\\ D_z\end{Bmatrix} = \begin{bmatrix} 0 & 0 & 0 & 0 & e_{15} & 0\\ 0 & 0 & 0 & e_{15} & 0 & 0\\ e_{31} & e_{31} & e_{33} & 0 & 0 & 0\end{bmatrix}\begin{Bmatrix}\varepsilon_{rr} - \alpha_1 T\\ \varepsilon_{\theta\theta} - \alpha_1 T\\ \varepsilon_{zz} - \alpha_3 T\\ \gamma_{\theta z}\\ \gamma_{rz}\\ \gamma_{r\theta}\end{Bmatrix} \\ + \begin{bmatrix}\eta_{11} & 0 & 0\\ 0 & \eta_{11} & 0\\ 0 & 0 & \eta_{33}\end{bmatrix}\begin{Bmatrix}E_r\\ E_\theta\\ E_z\end{Bmatrix}\end{gathered} \tag{9}$$

In which; η_{nn} indicate dielectric coefficients respectively. The components of electric field are considered as follows:

$$\{E_r \, , E_z \} = -\left\{\frac{\partial}{\partial r}, \frac{\partial}{\partial z}\right\}\varphi(r,z) \tag{10}$$

$$E_\theta = 0 \tag{11}$$

In which; $\varphi(r,z)$ is to represent electric potential

distribution in terms of radial and axial coordinates. The electric potential in the circumferential direction becomes zero due to the symmetry of the problem. In addition, electric potential distribution along the radial and axial directions is expressed as (Arefi and Zenkour 2017a, b):

$$\varphi(r,z) = \frac{2z}{h_0}\varphi_0 - \varphi(r)\cos(\frac{\pi z}{h_0}) \tag{12}$$

In which; φ_0 is applied electric potential and $\varphi(r)$ is considered a function that must be derived using electrical boundary conditions. Based on electric potential defined in Eq. (12), electric field components are defined as:

$$\begin{Bmatrix} E_r \\ E_z \end{Bmatrix} = \begin{Bmatrix} \varphi'(r)\cos(\frac{\pi z}{h_0}) \\ -(\frac{2\varphi_0}{h_0} + \frac{\pi}{h_0}\sin(\frac{\pi z}{h_0}))\varphi(r) \end{Bmatrix} \tag{13}$$

Substitution of electric fields and strains into constitutive relations leads to the following relations:

$$\begin{aligned} \sigma_r = {} & C_{11}(z)\cdot\big(u'(r) + z\psi'(r)\big) \\ & + \frac{C12(z)}{r}\big(u(r) + z\psi(r)\big) \\ & - \big(C_{11}(z) + C_{12}(z)\big)\big(\alpha_1(z)\cdot T(r)\big) \\ & - \big(C_{13}(z)\alpha_3(z)\cdot T(r)\big) \\ & + e_{31}(z)\left(\frac{2\varphi_0}{h_0}\right) \\ & + e_{31}(z)(\frac{\pi}{h_0}\sin\left(\frac{\pi z}{h_0}\right))\varphi(r) \end{aligned} \tag{14}$$

$$\begin{aligned} \sigma_\theta = {} & C_{12}(z)\cdot\big(u'(r) + z\psi'(r)\big) \\ & + \frac{C11(z)}{r}\big(u(r) + z\psi(r)\big) \\ & - \big(C_{11}(z) + C_{12}(z)\big)\big(\alpha_1(z)\cdot T(r)\big) \\ & - \big(C_{13}(z)\alpha_3(z)\cdot T(r)\big) \\ & + e_{31}(z)\left(\frac{2\varphi_0}{h_0}\right) \\ & + e_{31}(z)(\frac{\pi}{h_0}\sin\left(\frac{\pi z}{h_0}\right))\varphi(r) \end{aligned} \tag{15}$$

$$\begin{aligned} \sigma_{rz} = {} & C_{55}(z)\cdot\big(\psi(r) + w'(r)\big) \\ & + e_{15}(z)\cos(\frac{\pi z}{h_0})\varphi'(r) \end{aligned} \tag{16}$$

$$D_r = e_{15}(z)\big(\psi(r) + w'(r)\big) + \eta_{11}\varphi'(r)\,cos(\frac{\pi z}{h_0}) \tag{17}$$

$$\begin{aligned} D_z = {} & e_{31}(z)\big(u'(r) + z\psi'(r) - \alpha_1(z)\cdot T(r)\big) \\ & + \frac{e31(z)}{r}\big(u(r) + z\psi(r) - \alpha_1(z) \\ & \cdot T(r)\big) + e_{33}\big(-\alpha_3(z)\cdot T(r)\big) \\ & - \eta_{33}(\frac{2\varphi_0}{h_0} + \frac{\pi}{h_0}\sin(\frac{\pi z}{h_0}))\varphi(r) \end{aligned} \tag{18}$$

After the evaluation of the stresses conducted, the electric displacement and strain and the total potential energy of the system can be calculated using:

$$\Pi = U - W \tag{19}$$

Where U is the strain energy and is obtained by:

$$U = \frac{1}{2}\int\big(\sigma_{ij}\varepsilon_{ij} - D_iE_i\big)\,dV \tag{20}$$

The extension of stress and electric displacement components and definition of volume element leads to following relation for strain energy:

$$\begin{aligned} U = \pi\int_{r_i}^{r_o}\int_{-\frac{h(r)}{2}}^{\frac{h(r)}{2}} & [\,\sigma_r\varepsilon_r + \sigma_\theta\varepsilon_\theta + \sigma_{rz}\gamma_{rz} - D_rE_r \\ & - D_zE_z\,]\,rdrdz \end{aligned} \tag{21}$$

In addition, the work W performed by external work due to centrifugal force is defined as:

$$W = -\int_{r_i}^{r_o}\int_{-\frac{h(r)}{2}}^{\frac{h(r)}{2}}(2\pi\rho r^2\omega^2 u_r)drdz \tag{22}$$

Substitution of strain energy and external work into the total potential energy equation leads to the following relation:

$$\Pi = \int_{r_i}^{r_o} F(u,\psi,w,\varphi,r)\,dr \tag{23}$$

Where; $F(u,\psi,w,\varphi,r)$ is assumed to be the energy functional of the system. By substituting the stresses, strains and electric displacements in terms of displacements and electric potential, the energy functional can be derived as:

$$\begin{aligned} F(u,\psi,w,\varphi,r) = {} & A_{11}u'^2 + A_{12}\psi'^2 + A_{13}\psi'u' \\ & + A_{14}uu' + A_{15}\psi u' + A_{16}\psi'u \\ & + A_{17}\psi\psi' + A_{18}u' + A_{19}\psi' \\ & + A_{20}u'\varphi + A_{21}\psi'\varphi + A_{22}u' \\ & + A_{23}\psi' + A_{24}u' + A_{25}\psi' + A_{26}u'u \\ & + A_{27}\psi u' + A_{28}u\psi' + A_{29}\psi\psi' \\ & + A_{30}u^2 + A_{31}\psi u + A_{32}\psi^2 + A_{33}u \\ & + A_{34}\psi + A_{35}u\varphi + A_{36}\varphi\psi + A_{37}u \\ & + A_{38}\psi + A_{39}u + A_{40}\psi + A_{41}\psi^2 \\ & + A_{40}\psi w' + A_{43}w'^2 + A_{44}\varphi' \\ & + A_{45}\psi\varphi' + A_{46}w'\varphi' + A_{47}\varphi'^2 \\ & + A_{48}u' + A_{49}\psi' + A_{50}u'\varphi \\ & + A_{51}\psi'\varphi + A_{52}u + A_{53}\psi + A_{54}\varphi u \\ & + A_{55}\varphi\psi + A_{56}\varphi + A_{57}\varphi + A_{58}\varphi \\ & + A_{59} + A_{60} + A_{61}u' + A_{62}w \\ & + A_{63}\varphi^2 \end{aligned} \tag{24}$$

Where; A_{ij} represent the integration coefficients described in the appendix. Euler equations can be employed to obtain the final governing differential equation of the system (Arefi and Rahimi 2012)

$$\begin{cases} \frac{\partial F}{\partial u} - \left(\frac{\partial F}{\partial u'}\right)' = 0 \\ \frac{\partial F}{\partial w} - \left(\frac{\partial F}{\partial w'}\right)' = 0 \\ \frac{\partial F}{\partial \psi} - \left(\frac{\partial F}{\partial \psi'}\right)' = 0 \\ \frac{\partial F}{\partial \varphi} - \left(\frac{\partial F}{\partial \varphi'}\right)' = 0 \end{cases} \tag{25}$$

Eq. (25) in expanded form can be expressed as:

$$eq.A := \frac{\partial F}{\partial u} - \left(\frac{\partial F}{\partial u'}\right)' = 0$$

$$\begin{gathered} A_{16}\psi' + A_{28}\psi' + 2A_{30}u + A_{31}\psi + A_{33} + \\ A_{35}\varphi + A_{37} + A_{37} + A_{39} + A_{52} + A_{54}\varphi - 2A_{11}u'' - \\ 2A_{11}{}'u' - A_{13}\psi'' - A_{13}{}'\psi' - A_{14}{}'u - A_{15}\psi' - \\ A_{15}{}'\psi - A_{18}{}' - A_{20}\varphi' - A_{20}{}'\varphi - A_{22}{}' - A_{24}{}' - \\ A_{26}{}'u - A_{27}\psi' - A_{27}{}'\psi - A_{48}{}' - A_{50}\varphi' - A_{50}{}'\varphi - \\ A_{61}{}' = 0 \end{gathered} \tag{26}$$

$$eq.B := \frac{\partial F}{\partial \psi} - \left(\frac{\partial F}{\partial \psi'}\right)' = 0$$

$$\begin{gathered} A_{15}u' + A_{27}u' + A_{31}u + 2A_{32}\psi + A_{34} + A_{36}\varphi + A_{38} \\ + A_{40} + 2A_{41}\psi + A_{42}w' + A_{45}\varphi' \\ + A_{53} + A_{55}\varphi - 2A_{12}\psi'' - 2A_{12}{}'\psi' \\ - A_{13}u'' - A_{13}{}'u' - A_{16}u' - A_{16}{}'u \\ - A_{17}{}'\psi - A_{19}{}' - A_{21}\varphi' - A_{21}{}'\varphi \\ - A_{23}{}' - A_{25}{}' - A_{28}u' - A_{28}{}'u \\ - A_{29}{}'\psi - A_{49}{}' - A_{51}\varphi' - A_{51}{}'\varphi = \end{gathered} \tag{27}$$

$$\begin{gathered} eq.C := \frac{\partial F}{\partial w} - \left(\frac{\partial F}{\partial w'}\right)' = 0 \\ -A_{62} + A_{42}\psi' + A_{42}{}'\psi + 2A_{43}w'' + \\ 2A_{43}{}'w' + A_{46}\varphi'' + A_{46}{}'\varphi' = 0 \end{gathered} \tag{28}$$

$$eq.D := \frac{\partial F}{\partial \varphi} - \left(\frac{\partial F}{\partial \varphi'}\right)' = 0$$

$$\begin{gathered} 2A_{63}\varphi + A_{20}u' + A_{21}\psi' + A_{35}u + A_{36}\psi + A_{50}u' \\ + A_{51}\psi' + A_{54}u + A_{55}\psi + A_{56} \\ + A_{57} + A_{58} - A_{44}{}' - A_{45}\psi' \\ - A_{45}{}'\psi - 2A_{47}\varphi'' - 2A_{47}{}'\varphi' \\ - A_{46}w'' - A_{46}{}'w' = 0 \end{gathered} \tag{29}$$

Stress resultants need to be calculated in order to impose the boundary conditions. The stress resultant relations are as follows:

$$(N_r, N_\theta, Q_r) = \int_{-\frac{h(r)}{2}}^{\frac{h(r)}{2}} (\sigma_r, \sigma_\theta, \sigma_{rz}) dz \tag{30}$$

$$(M_r, M_\theta) = \int_{-\frac{h(r)}{2}}^{\frac{h(r)}{2}} (\sigma_r, \sigma_\theta) z dz \tag{31}$$

$$\begin{gathered} N_r = I_{01}u' + I_{02}\psi' + I_{03}u + I_{04}\psi + I_{05} + I_{06}\varphi + I_{07} \\ + I_{08} \end{gathered} \tag{32}$$

$$\begin{gathered} M_r = I_{11}u' + I_{12}\psi' + I_{13}u + I_{14}\psi + I_{15} + I_{16}\varphi + I_{17} \\ + I_{18} \end{gathered} \tag{33}$$

$$Q_r = I_{21}w' + I_{21}\psi + I_{22}\varphi' \tag{34}$$

Where; I_{mn} represents integration coefficients, which are described in the appendix. The Boundary conditions for a clamped-free disk can be expressed as:

$$r = r_i: \quad u = 0\,,\ \psi = 0\,,\ w = 0\,,\ \varphi = 0 \tag{35}$$

$$r = r_o: \quad N_r = 0\,,\ M_r = 0\,,\ Q_r = 0\,, \varphi = 0 \tag{36}$$

5. Solution procedure

The formulated Eq. (25) and the following boundary conditions are taken as a system of ODEs that govern the displacement field of the disk. These equations were solved numerically by Maple Software with the numerical option. Refined mesh was also applied to increase efficiency. The Stresses were then calculated directly from the displacement field.

In this research, the FEM modelling was used to validate the results using the Abaqus Software. The disk was modeled by revolving a thickness profile. Thereafter, material properties were applied by introducing piezoelectric coefficients and engineering stiffness constants. The electric and displacement boundary conditions as well as body forces were implemented in the model.

The piezoelectric mesh element C3D8E was applied to the disk with the mesh orientation adjusted for axial polarization of disk. Mesh refinements were also applied and the resulting electric potential is presented in Fig. 2. Element sizes varied from 0.5mm to 0.3mm so that 147270 elements were meshed.

6. Numerical results and discussions

Before presentation of full numerical results, the thermal, mechanical and electrical boundary conditions together with other conditions are expressed as:

- Constant angular velocity of 1000 rad/s
- Zero electric potential at the inner and outer radius of the disk
- Disk is clamped in the inner radius and has zero degrees of freedom
- Free at the outer radius (six degrees of freedom)

In this study, the governing Eqs. (25)-(27) were numerically solved using MAPLE18 Software. Material properties implemented in this analysis are presented in Table 1. In this section, the effect of various parameters such as root thickness to inner radius ratio ($\frac{h_0}{r_i}$), outer to inner radius ratio ($\frac{r_o}{r_i}$), profile thickness index (m) and gradation index (n) on radial stress and electric potential have been presented.

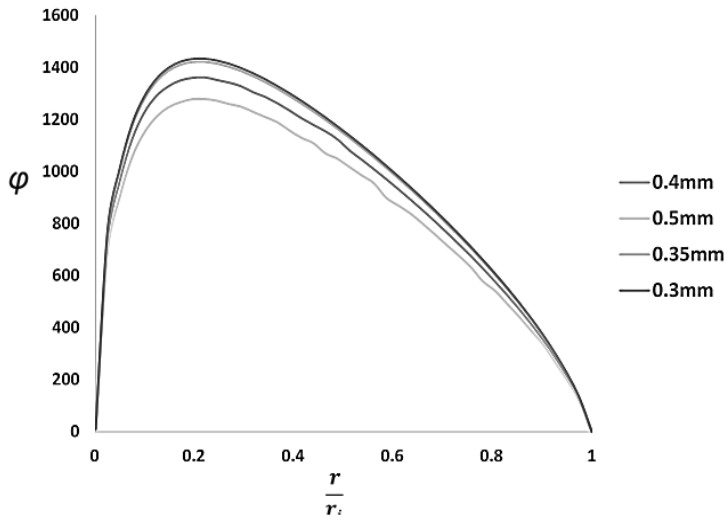

Fig. 2 Effect of various mesh sizes

Table 1 PZT Material Properties

Parameter	*PZT-4*	*PZT-5A*
C_{11}	$139\ GPa$	$121\ GPa$
C_{12}	$77.8\ GPa$	$75.9\ GPa$
C_{13}	$74\ GPa$	$75.4\ GPa$
C_{33}	$115\ GPa$	$111\ GPa$
C_{55}	$25.6\ GPa$	$21.1\ GPa$
e_{31}	$-5.2\ {}^{C}/_{m^2}$	$-5.4\ {}^{C}/_{m^2}$
e_{33}	$15.1\ {}^{C}/_{m^2}$	$15.8\ {}^{C}/_{m^2}$
e_{15}	$12.7\ {}^{C}/_{m^2}$	$12.3\ {}^{C}/_{m^2}$
η_{11}	$0.646 \times 10^{-8}\ {}^{C}/_{\mathrm{vm}}$	$0.811 \times 10^{-8}\ {}^{C}/_{\mathrm{vm}}$
η_{33}	$0.562 \times 10^{-8}\ {}^{C}/_{\mathrm{vm}}$	$0.735 \times 10^{-8}\ {}^{C}/_{\mathrm{vm}}$
α_1	$3.8 \times 10^{-6}\ {}^{1}/_{C^\circ}$	$1.2 \times 10^{-6}\ {}^{1}/_{C^\circ}$
α_3	$1.7 \times 10^{-6}\ {}^{1}/_{C^\circ}$	$4 \times 10^{-6}\ {}^{1}/_{C^\circ}$
K	$1.25\ {}^{W}/_{mC^\circ}$	$1.25\ {}^{W}/_{mC^\circ}$
ρ	$7800\ {}^{kg}/_{m^3}$	$7800\ {}^{kg}/_{m^3}$

6.1 Effects of $\frac{h_0}{r_i}$ ratio

Figure 3(a) indicates the variation of the maximum electric potential for different $\frac{h_0}{r_i}$. The electric potential is zero at the inner and outer radiuses which satisfies the boundary conditions. It can also be observed that the electric potential increases dramatically as the $\frac{h_0}{r_i}$ ratio increases.

Normalized radial stress for various $\frac{h_0}{r_i}$ is shown in Fig. 3(b). It is noticeable that the stress levels depict a sharp increase as $\frac{h_0}{r_i}$ decreases. The radial stress values reduce to zero at the outer radius as we expected, since it is a stress-free surface. It should also be noted that the radial stress undergoes a strong increase adjacent to the inner radius. This behavior cannot be observed for lower values of $\frac{h_0}{r_i}$.

Generally, the local concentration of strains develop electric potential. Higher $\frac{h_0}{r_i}$ will result in an increase of stresses and strains and therefore affect the electric potential. Therefore the increase of stress near the inner radius justifies the electric potential peak in that area.

6.2 Effect of $\frac{r_o}{r_i}$ ratio

The maximum electric potential and the normalized radial stress values with respect to the dimensionless radius for various $\frac{r_o}{r_i}$ ratios are illustrated in Figs. 4(a)-(b). An increase in the electric potential with the increase of the $\frac{r_o}{r_i}$ ratio is observed in Fig. 4(a). It has been observed that the electric potential peak relocates towards the inner radius as

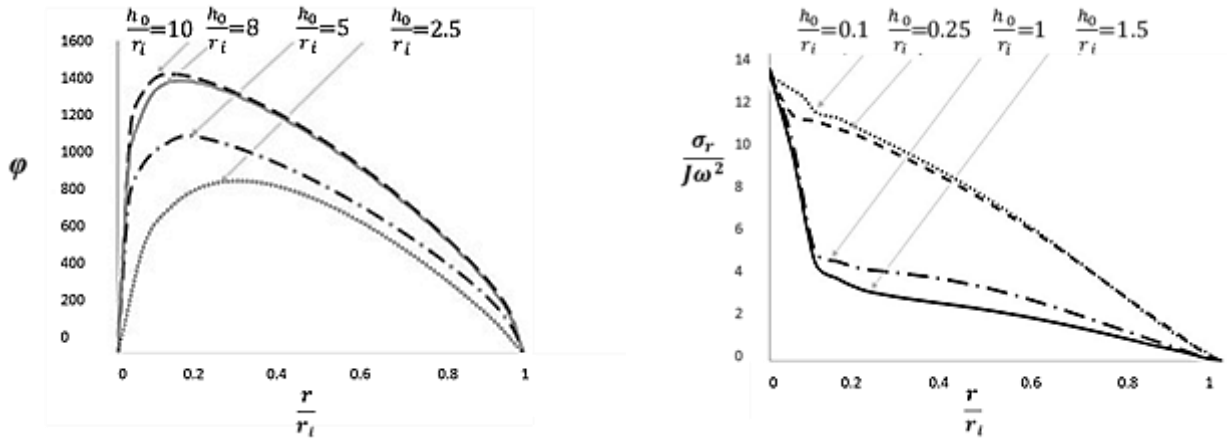

(a) Maximum electric potential (b) Normalized radial stress

Fig. 3 Effect of various thickness ratios

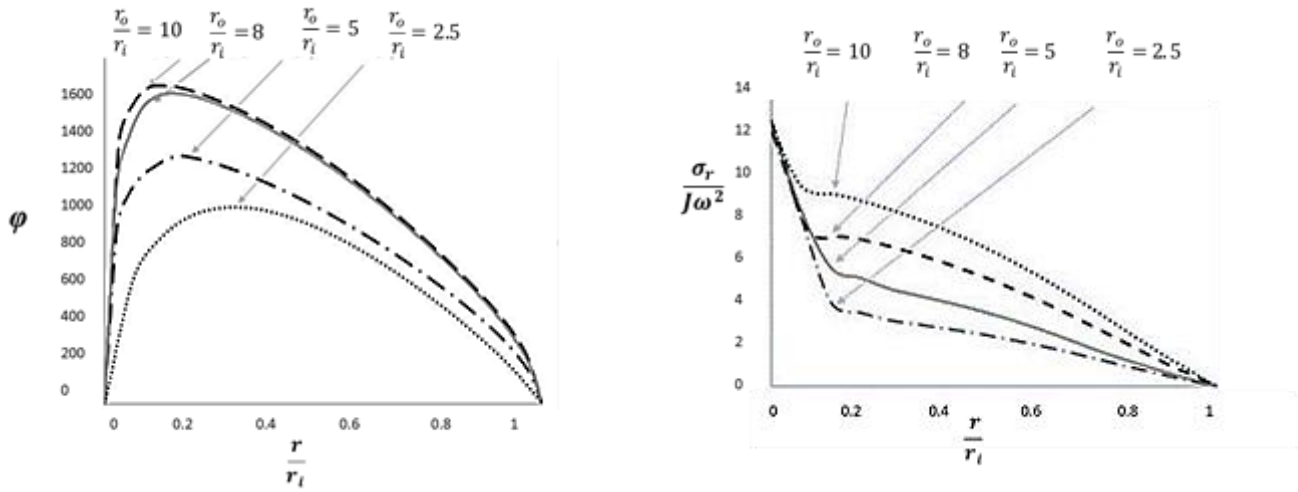

(a) Maximum Electric Potential (b) Normalized Radial Stress

Fig. 4 Effect of various radius ratios

$\frac{r_o}{r_i}$ increases. Fig. 4(b) illustrates the normalized radial stress for the same ratios.

It can be perceived that increasing the $\frac{r_o}{r_i}$ ratio will result in a decrease in the radial stress as also reported for isotropic materials (Afsar and Go 2010)..

6.3 Gradation index

Figs. 4(a)-(b) represent the electric potential stress and normalized radial stress for different grading indices. It can be seen from figure 7 that increasing the grading index of n results in a higher radial stress. Higher electric potentials can also be observed associated with this grading index.

A higher grading index results in a sharper gradation from PZT5 to PZT4. Furthermore, increasing the grading index will result in a higher PZT5 volume fraction. PZT5 properties have higher dielectric coefficients and therefor influence the developed electric field more than expected values. However PZT5 has higher piezoelectric coefficients than that of PZT4 thus the increase in stress is also obtained due to the coupling.

6.4 Thickness profile

The electric potential for various profile thicknesses is presented in Fig. 6. It is noticeable that for profile $m = 4$ a small increase of 60 volts can be observed. No noticeable changes on stress with various profile thicknesses were concluded.

6.5 Rotation speeds

The electric potential for different rotation speeds is illustrated in Fig. 7. Increasing the rotation speed will result in a rise of the electric potential. This is just as we expected since it would result in a higher radial stress and strain. The higher rotation speeds will generally generate more electric potential in the FGP disk.

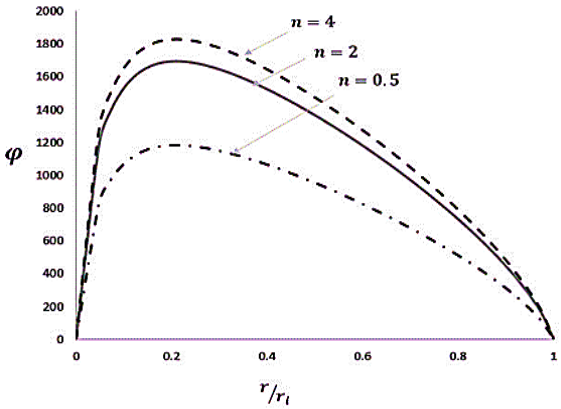

(a) Maximum Electric Potential

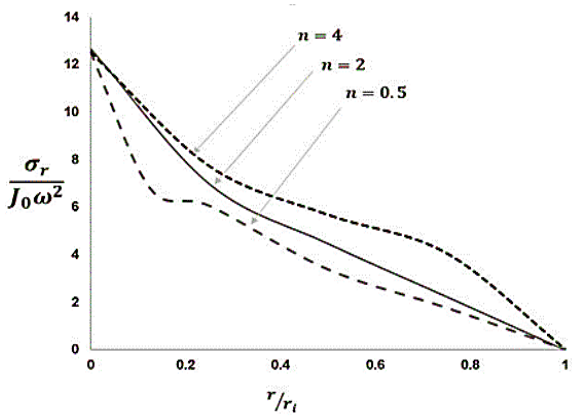

(b) Normalized Radial Stress

Fig. 5 Effect of various gradation index values

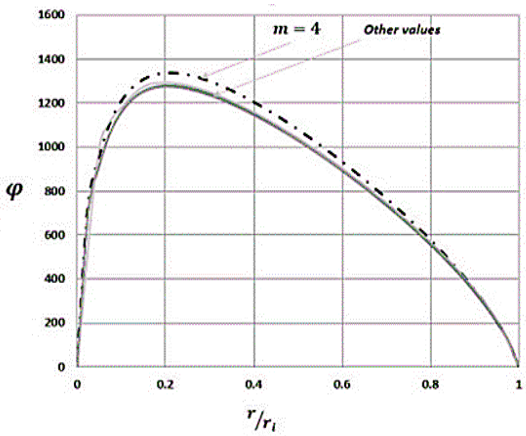

Fig. 6 Effect of various gradation index values

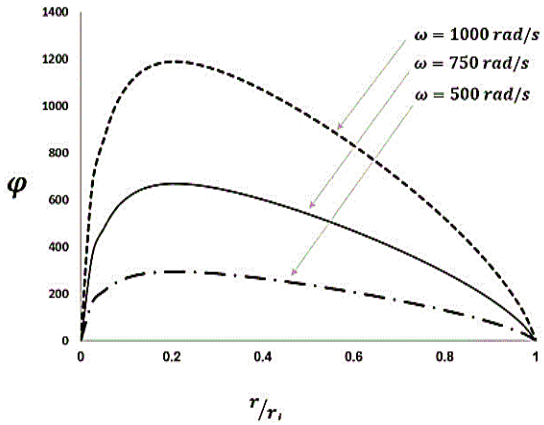

Fig. 7 Effect of various gradation index values

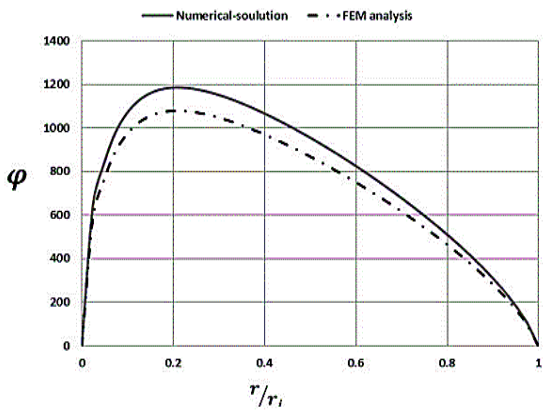

Fig. 8 Comparison between results from FEM and Numerical Method

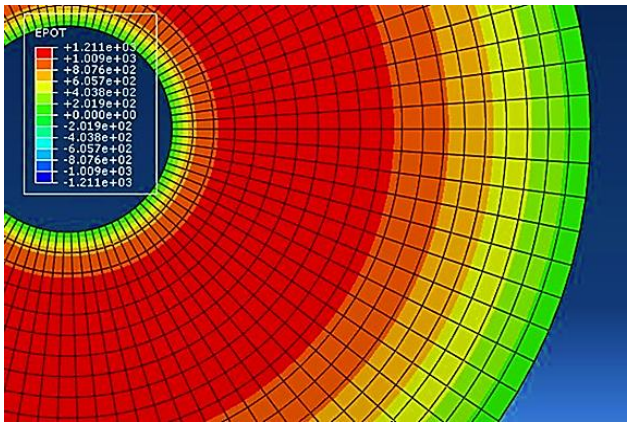

Fig. 9 FEM Electric Potential Contours for the simulated disk

The numerical analysis carried out in this study were validated by FEM analysis using the ABAQUS CAE Software. Validation of the electric potential with the FEM results is presented in Fig. 8. Fig. 9, displays the electric potential contour in this analysis.

The maximum error between FEM results and the numerical analysis was less than 9.8% in all cases and thus acceptable agreement is achieved.

7. Conclusions

Numerical and FEM analysis were performed to obtain the electric potential, displacements and radial stresses for a variable thickness FGP rotating disk with axial polarization under thermal and mechanical loading. Principles of virtual displacement was used to derive governing equations of electro-elastic bending. Thermal conductivity equation was

solved for a functionally graded material. The variable thickness disk was subjected to applied electric potential. Various $\frac{r_o}{r_i}$, $\frac{h_0}{r_i}$, profile thickness and grading indices were considered by holding constant for all other parameters.

- This study has concluded that an increase in $\frac{h_0}{r_i}$ ratio will result in a higher electric potential. However, a higher $\frac{h_0}{r_i}$ ratio will result in a lower normalized stress level due to the smaller rotational inertia.
- An increase in $\frac{r_o}{r_i}$ ratio will result in a rise in the electric potential but will lower the normalized radial stress.
- No dramatic changes with various thickness profiles were observed. However, the profile thickness index $(m = 4)$ experienced an increase in the electric potential by up to 5%.
- Lower grading indices produce lower strains due
- to the increase in the overall stiffness of the disk thus, decreasing the maximum electric potential. A small decrease in the radio stress could also be observed by lowering the grading index.

References

Afsar, A. and Go, J. (2010), "Finite element analysis of thermoelastic field in a rotating FGM circular disk", *Appl. Math Modelling,* **34**(11), 3309-3320. https://doi.org/10.1016/j.apm.2010.02.022

Arefi, M. and Rahimi, G. H. (2013), "Thermo elastic analysis of a functionally graded cylinder under internal pressure using first order shear deformation theory", *Sci. Res. Essays.,* **5**(12), 1442-1454.

Arefi, M. and Rahimi, G. (2011), "Nonlinear analysis of a functionally graded square plate with two smart layers as sensor and actuator under normal pressure", *Smart. Struct. Syst.,* **8**(5), 433-447. http://dx.doi.org/10.12989/sss.2011.8.5.433.

Arefi, M. and Rahimi, G. (2012), "Studying the nonlinear behavior of the functionally graded annular plates with piezoelectric layers as a sensor and actuator under normal pressure", *Smart. Struct. Syst*., **9**(2), 127-143. http://doi.org/10.12989/sss.2012.9.2.127.

Arefi, M., Rahimi, G.H. and Khoshgoftar, M.J. (2012), "Exact solution of a thick walled functionally graded piezoelectric cylinder under mechanical, thermal and electrical loads in the magnetic field", *Smart. Struct. Syst*., **9**(5), 427-439. http://doi.org/10.12989/sss.2012.9.5.427.

Arefi, M. and Rahimi, G. (2012), "Three-dimensional multi-field equations of a functionally graded piezoelectric thick shell with variable thickness, curvature and arbitrary nonhomogeneity", *Acta. Mech.,* **223**(1), 63-79. https://doi.org/10.1007/s00707-011-0536-5.

Arefi, M. and Rahimi, G.H. (2014), "Comprehensive piezo-thermo-elastic analysis of a thick hollow spherical shell", *Smart. Struct. Syst.,* **14**(2), 225-246. http://doi.org/10.12989/sss.2014.14.2.225.

Arefi, M. and Allam, M.N.M., (2015), "Nonlinear Responses of an Arbitrary FGP Circular Plate Resting on Foundation", *Smart. Struct. Syst.,* **16**(1), 81-100. http://dx.doi.org/10.12989/sss.2015.16.1.081.

Arefi, M., Rahimi, G.H. and Khoshgoftar, M.J. (2011), "Optimized design of a cylinder under mechanical, magnetic and thermal loads as a sensor or actuator using a functionally graded piezomagnetic material", *Int. J. Phys. Sci*., **6**(27), 6315-6322.

Arefi, M. (2015), "Nonlinear electromechanical analysis of a functionally graded square plate integrated with smart layers resting on Winkler-Pasternak foundation", *Smart. Struct. Syst.,* **16**(1), 195-211. https://doi.org/10.12989/sss.2015.16.1.195.

Arefi, M. and Zenkour, A.M. (2017a), "Effect of thermo-magneto-electro-mechanical fields on the bending behaviors of a three-layered nanoplate based on sinusoidal shear-deformation plate theory", *J. Sandw. Struct. Mater*. https://doi.org/10.1177/1099636217697497.

Arefi, M. and Zenkour, A.M. (2017b), "Employing the coupled stress components and surface elasticity for nonlocal solution of wave propagation of a functionally graded piezoelectric Love nanorod model", *J. Intel. Mater. Syst. Struct.,* **28**(17), 2403-2413. https://doi.org/10.1177/1045389X17689930.

Bayat, M., Sahari, B., Saleem, M., Aidy, A. and Wong, S. (2009), "Bending analysis of a functionally graded rotating disk based on the first shear deformation theory", *Appl. Math. Modeling.,* **33**(11), 4215-4230. https://doi.org/10.1016/j.apm.2009.03.001.

Bayat, M., Sahari, B., Saleem, M., Hambouda, A. and Mahdi, E. (2007), "Thermoelastic analysis of a functionally graded rotating disk with small and large deflections", *Thin. Wall. Struct.,* **45**(7), 677-691. https://doi.org/10.1016/j.tws.2007.05.005.

Chen, J., Ding, H. and Chen, W. (2007), "Three-dimensional analytical solution for a rotating disc of functionally graded materials with transverse isotropy", *Arch. Appl. Mech.,* **77**(4), 241-251. https://doi.org/10.1007/s00419-006-0098-5.

Dai, H. and Dai, H. (2017), "Analysis of a rotating FGMME circular disk with variable thickness under thermal environment", *Appl. Math. Modelling.,* **45**, 900-924. https://doi.org/10.1016/j.apm.2017.01.007.

Durodola, J. and Attia, O. (2000), "Deformations and stresses in functionally graded graded rotating disks", *Compos. Sci. Tech.,* **60**(7), 897-995. https://doi.org/10.1016/S0266-3538(99)00197-9.

Durodola, J. and Attia, O. (2000), "Property gradation for modification response of rotating MMC discs", *Mater. Sci. Tech.,* **16**(7-8), 919-924. https://doi.org/10.1179/026708300101508694.

Ghasemi, H., Park, H.S. and Rabczuk, T. (2018), "A multi-material level set based topology optimization of flexoelectric composites", *Comput. Meth. Appl. Mech. Eng.,* **332**, 47-62. https://doi.org/10.1016/j.cma.2017.12.005.

Ghasemi, H., Park, H. and Rabczuk, T. (2017), "A leve-set based IGA formulation for topology optimization of flexoelectric materials", *Comput. Meth. Appl. Mech. Eng.,* **313**, 239-258. https://doi.org/10.1016/j.cma.2016.09.029.

Hamdia, K.M., Silani, M., Zhuang, X., He, P. and Rabczuk, T. (2017), "Stochastic analysis of the fracture toughness of polymeric nanoparticle composite using polynomial chaos expansion", *Int. J. Frac.,* **206**(2), 215-227. https://doi.org/10.1007/s10704-017-0210-6.

Holt, J., Koizumi, M., Hirai, T. and Munir, Z. (1993), "Ceramic transactions: Functionally Gradient Materials", *American Ceramic Soc.*, **34**.

Jahed, H. and Sherkatti, S. (2000), "Thermoplastic analysis of inhomogeneous rotating disk with variable thickness", *EMHS Conference of Fatigue,* Cambridge, Untied Kingdom, April.

Kheirkhah, S. and Loghman, A. (2015), "Electric potential redistribution due to time dependent creep in thick walled FGPM cylinder based on Mendelson method of successive approximation", *Struct. Eng. Mech.,* **53**(6), 1167-1182. https://doi.org/10.12989/sem.2015.53.6.1167.

Li, X., Ding, H. and Chen, W. (2006), "Pure bending of a simply supported circular plate of transversely isotropic functionally graded material", *J. Zhej. Uni. Sci.,* **A7**(8), 1324-1328. https://doi.org/10.1631/jzus.2006.A1324.

Li, X., Ding, H. and Chen, W. (2008), "Elasticity solutions for a

transversely isotropic functionally graded circular plate subject to an axisymmetric transverse load qr K", *Int. J. Solids. Struct.,* **45**(1), 191-210. https://doi.org/10.1016/j.apm.2010.02.022.

Loghman, A., Abdollahian, M., Jazi, A. and Arani, A. (2013), "Semi-analytical solution for electromagne to thermoelastic creep response of a functionally graded piezo-electric rotating disk", *Int. J. Therm. Sci.,* **65**, 254-266. https://doi.org/10.1016/j.ijthermalsci.2012.10.011.

Nanthakumar, S., Lahmer, T., Zhuang, X., Zi, G. and Rabczuk, T. (2016), "Detection of material interfaces using a regularized level set method in piezoelectric structures", *Inv. Prob. Sci. Eng.,* **24**(1), 153-176. https://doi.org/10.1080/17415977.2015.1017485.

Nguyen, B., Nanthakumar, S., Zhuang, X., Wriggers, P., Jiang, X. and Rabczuk, T. (2018), "Dynamic flexoelectric effect on piezoelectric nanostructures", *Euro. J. Mech.- A/Solids,* **71**, 404-409. https://doi.org/10.1016/j.euromechsol.2018.06.002.

Nguyen, B., Zhuang, X. and Rabczuk, T. (2018), "Numerical model for the characterization of Maxwell-Wagner relaxation in piezoelectric and flexoelectric composite material", *Comput. Struct.,* **208**, 75-91. https://doi.org/10.1016/j.compstruc.2018.05.006.

Deneva, P., Gross, D., Muller, R. and Rangelov, T. (2014), *Dynamic Fracture of Piezoelectric Materials*, Springer, Germany.

Parveen, G. and Reddy, J. (1998), "Nonlinear transient thermoelastic analysis of functionally graded ceramic-metal plates", *Int. J. Solids. Struct.,* **35**(33), 4457-4476. https://doi.org/10.1016/S0020-7683(97)00253-9.

Reddy, J. (2000), "Analysis of functionally graded plates", *Int. J. Numer. Meth. Eng.,* **47**(1-3), 663-684.

Reddy, J., Wang, C. and Kitipornchai, S. (1999), "Axisymmetric bending of a functionally graded circular and annular plare", *J. Mech.-A/solids,* **18**(2), 185-199. https://doi.org/10.1016/S0997-7538(99)80011-4.

Suresh, S. and Mortensen, A. (1998), *Fundamentals of Functionally Graded Materials*, The Institute of Materials, United Kingdom.

Thai, T., Rabczuk, T. and Zhuang, X. (2018), "A large deformation isogeometric approach for flexoelectric and soft materials", *Comput. Meth. Appl. Eng.,* **341**, 718-739.

Vu Bac, N., Lahmer, T., Zhuang, X., Nguyen-Thoi, T. and Rabczuk, T. (2016), "A software framework for probabilistic sensitivity analysis for computational expensive models", *Adv. Eng. Soft.,* **100**, 19-31. https://doi.org/10.1016/j.advengsoft.2016.06.005

Zenkour, A. and Mashat, D. (2011), "Stress function of a variable-thickness annular disk using exact and numerical methods", *Engineering.,* **3**(04), 422. https://:10.4236/eng.2011.34048.

CC

Appendix: Integration Coefficients

$$A_{11} = \int_{-\frac{h(r)}{2}}^{\frac{h(r)}{2}} [\pi r C_{11}(z)] dz$$

$$A_{12} = \int_{-\frac{h(r)}{2}}^{\frac{h(r)}{2}} [\pi r C_{11}(z) z^2] dz$$

$$A_{13} = \int_{-\frac{h(r)}{2}}^{\frac{h(r)}{2}} [2\pi r C_{11}(z) z] dz$$

$$A_{14} = \int_{-\frac{h(r)}{2}}^{\frac{h(r)}{2}} [\pi C_{12}(z)] dz$$

$$A_{15} = \int_{-\frac{h(r)}{2}}^{\frac{h(r)}{2}} [\pi r C_{12}(z) z] dz$$

$$A_{16} = \int_{-\frac{h(r)}{2}}^{\frac{h(r)}{2}} [\pi C_{12}(z) z] dz$$

$$A_{17} = \int_{-\frac{h(r)}{2}}^{\frac{h(r)}{2}} [\pi C_{12}(z) z^2] dz$$

$$A_{18} = \int_{-\frac{h(r)}{2}}^{\frac{h(r)}{2}} \left[\pi r \cdot e_{31}(z) \frac{2\pi}{h_0}\right] dz$$

$$A_{19} = \int_{-\frac{h(r)}{2}}^{\frac{h(r)}{2}} \left[z\pi r \cdot e_{31}(z) \frac{2\pi}{h_0}\right] dz$$

$$A_{20} = \int_{-\frac{h(r)}{2}}^{\frac{h(r)}{2}} \left[\pi r \cdot e_{31}(z) \frac{\pi}{h_0} \sin(\frac{\pi z}{h_0})\right] dz$$

$$A_{21} = \int_{-\frac{h(r)}{2}}^{\frac{h(r)}{2}} \left[\pi z r \cdot e_{31}(z) \frac{\pi}{h_0} \sin(\frac{\pi z}{h_0})\right] dz$$

$$A_{22} = \int_{-\frac{h(r)}{2}}^{\frac{h(r)}{2}} [\pi r(-\alpha_1(z)T(r))(C11(z) + C_{12}(z))] dz$$

$$A_{23} = \int_{-\frac{h(r)}{2}}^{\frac{h(r)}{2}} [\pi r z(-\alpha_1(z)T(r))(C11(z) + C_{12}(z))] dz$$

$$A_{24} = \int_{-\frac{h(r)}{2}}^{\frac{h(r)}{2}} [\pi r(-\alpha_3(z)T(r))(C_{13}(z))] dz$$

$$A_{25} = \int_{-\frac{h(r)}{2}}^{\frac{h(r)}{2}} [\pi r z(-\alpha_3(z)T(r))(C_{13}(z))] dz$$

$$A_{26} = \int_{-\frac{h(r)}{2}}^{\frac{h(r)}{2}} [\pi C_{12}(z)] dz$$

$$A_{27} = \int_{-\frac{h(r)}{2}}^{\frac{h(r)}{2}} [\pi z C_{12}(z)] dz$$

$$A_{28} = A_{27}$$

$$A_{29} = \int_{-\frac{h(r)}{2}}^{\frac{h(r)}{2}} [\pi z^2 C_{12}(z)] dz$$

$$A_{30} = \int_{-\frac{h(r)}{2}}^{\frac{h(r)}{2}} \left[\pi \frac{C_{11}(z)}{r}\right] dz$$

$$A_{31} = \int_{-\frac{h(r)}{2}}^{\frac{h(r)}{2}} \left[\pi z \frac{2C_{11}(z)}{r}\right] dz$$

$$A_{32} = \int_{-\frac{h(r)}{2}}^{\frac{h(r)}{2}} \left[\pi z^2 \frac{2C_{11}(z)}{r}\right] dz$$

$$A_{33} = \int_{-\frac{h(r)}{2}}^{\frac{h(r)}{2}} \left[\pi(\frac{2\varphi_0}{h_0}) e_{31}(z)\right] dz$$

$$A_{34} = \int_{-\frac{h(r)}{2}}^{\frac{h(r)}{2}} \left[\pi z(\frac{2\varphi_0}{h_0}) e_{31}(z)\right] dz$$

$$A_{35} = \int_{-\frac{h(r)}{2}}^{\frac{h(r)}{2}} \left[\pi r(\frac{\pi}{h_0}) e_{31}(z) \sin(\frac{\pi z}{h_0})\right] dz$$

$$A_{36} = \int_{-\frac{h(r)}{2}}^{\frac{h(r)}{2}} \left[\pi r z(\frac{\pi}{h_0}) e_{31}(z) \sin(\frac{\pi z}{h_0})\right] dz$$

$$A_{37} = \int_{-\frac{h(r)}{2}}^{\frac{h(r)}{2}} [\pi(-\alpha_1(z)T(r))(C11(z) + C_{12}(z))] dz$$

$$A_{38} = \int_{-\frac{h(r)}{2}}^{\frac{h(r)}{2}} [\pi z(-\alpha_1(z)T(r))(C11(z) + C_{12}(z))] dz$$

$$A_{39} = \int_{-\frac{h(r)}{2}}^{\frac{h(r)}{2}} [\pi(-\alpha_3(z)T(r))(C_{13}(z))] dz$$

$$A_{40} = \int_{-\frac{h(r)}{2}}^{\frac{h(r)}{2}} [\pi z(-\alpha_3(z)T(r))(C_{13}(z))] dz$$

$$A_{41} = \int_{-\frac{h(r)}{2}}^{\frac{h(r)}{2}} [\pi r C_{55}(z)] dz$$

$$A_{42} = 2A_{41}$$

$$A_{43} = A_{41}$$

$$A_{44} = \int_{-\frac{h(r)}{2}}^{\frac{h(r)}{2}} \left[-\pi r e_{15}(z)\cos(\frac{\pi z}{h_0})\right] dz$$

$$A_{45} = \int_{-\frac{h(r)}{2}}^{\frac{h(r)}{2}} \left[+\pi r e_{15}(z)\cos(\frac{\pi z}{h_0})\right] dz$$

$$A_{46} = A_{45}$$

$$A_{47} = \int_{-\frac{h(r)}{2}}^{\frac{h(r)}{2}} \left[\pi r \eta_{11}(z)\cos^2(\frac{\pi z}{h_0})\right] dz$$

$$A_{48} = \int_{-\frac{h(r)}{2}}^{\frac{h(r)}{2}} \left[-\pi r(\frac{2\pi}{h_0})e_{31}(z)\right] dz$$

$$A_{49} = \int_{-\frac{h(r)}{2}}^{\frac{h(r)}{2}} \left[-\pi r z(\frac{2\pi}{h_0})e_{31}(z)\right] dz$$

$$A_{50} = \int_{-\frac{h(r)}{2}}^{\frac{h(r)}{2}} \left[-\pi r(\frac{\pi}{h_0})e_{31}(z)\sin(\frac{\pi z}{h_0})\right] dz$$

$$A_{51} = \int_{-\frac{h(r)}{2}}^{\frac{h(r)}{2}} \left[-\pi r z(\frac{\pi}{h_0})e_{31}(z)\sin(\frac{\pi z}{h_0})\right] dz$$

$$A_{52} = \int_{-\frac{h(r)}{2}}^{\frac{h(r)}{2}} \left[-\pi r(\frac{2\pi}{h_0})e_{31}(z)\right] dz$$

$$A_{53} = \int_{-\frac{h(r)}{2}}^{\frac{h(r)}{2}} \left[-\pi r z(\frac{2\pi}{h_0})e_{31}(z)\right] dz$$

$$A_{54} = \int_{-\frac{h(r)}{2}}^{\frac{h(r)}{2}} \left[-\pi(\frac{\pi}{h_0})e_{31}(z)\sin(\frac{\pi z}{h_0})\right] dz$$

$$A_{55} = \int_{-\frac{h(r)}{2}}^{\frac{h(r)}{2}} \left[-\pi z(\frac{\pi}{h_0})e_{31}(z)\sin(\frac{\pi z}{h_0})\right] dz$$

$$A_{56} = \int_{-\frac{h(r)}{2}}^{\frac{h(r)}{2}} \left[\pi r(\frac{4\varphi_0\pi}{{h_0}^2})\eta_{33}(z)\sin(\frac{\pi z}{h_0})\right] dz$$

$$A_{57} = \int_{-\frac{h(r)}{2}}^{\frac{h(r)}{2}} \left[2\pi r e_{31}(z)\frac{\pi}{h_0}\sin(\frac{\pi z}{h_0})(\alpha_1(z)T(r))\right] dz$$

$$A_{58} = \int_{-\frac{h(r)}{2}}^{\frac{h(r)}{2}} \left[\pi r e_{31}(z)\frac{\pi}{h_0}\sin(\frac{\pi z}{h_0})(\alpha_3(z)T(r))\right] dz$$

$$A_{59} = \int_{-\frac{h(r)}{2}}^{\frac{h(r)}{2}} \left[2\pi r e_{31}(z)\frac{2\pi}{h_0}(\alpha_1(z)T(r))\right] dz$$

$$A_{60} = \int_{-\frac{h(r)}{2}}^{\frac{h(r)}{2}} \left[\pi r e_{33}(z)\frac{2\pi}{h_0}(\alpha_3(z)T(r))\right] dz$$

$$A_{61} = \int_{-\frac{h(r)}{2}}^{\frac{h(r)}{2}} [2\pi\rho(z)r^2\omega^2] dz$$

$$A_{62} = 2\pi r q_z$$

$$I_1 = \int_{-\frac{h(r)}{2}}^{\frac{h(r)}{2}} [C_{11}(z)] dz$$

$$I_2 = \int_{-\frac{h(r)}{2}}^{\frac{h(r)}{2}} [zC_{11}(z)] dz$$

$$I_3 = \int_{-\frac{h(r)}{2}}^{\frac{h(r)}{2}} \left[\frac{C_{12}(z)}{r}\right] dz$$

$$I_4 = \int_{-\frac{h(r)}{2}}^{\frac{h(r)}{2}} \left[z\frac{C_{12}(z)}{r}\right] dz$$

$$I_5 = \int_{-\frac{h(r)}{2}}^{\frac{h(r)}{2}} \left[\frac{2\pi}{h_0}e_{31}(z)\right] dz$$

$$I_6 = \int_{-\frac{h(r)}{2}}^{\frac{h(r)}{2}} \left[\frac{\pi}{h_0}e_{31}(z)\sin(\frac{\pi z}{h_0})\right] dz$$

$$I_7 = \int_{-\frac{h(r)}{2}}^{\frac{h(r)}{2}} [(C_{11}(z) + C_{12}(z))(-\alpha_1(z)T(r))] dz$$

$$I_8 = \int_{-\frac{h(r)}{2}}^{\frac{h(r)}{2}} [C_{13}(z)(-\alpha_3(z)T(r))] dz$$

$$I_{11} = \int_{-\frac{h(r)}{2}}^{\frac{h(r)}{2}} [zC_{11}(z)] dz$$

$$I_{12} = \int_{-\frac{h(r)}{2}}^{\frac{h(r)}{2}} [z^2C_{11}(z)] dz$$

$$I_{13} = \int_{-\frac{h(r)}{2}}^{\frac{h(r)}{2}} \left[z\frac{C_{12}(z)}{r}\right] dz$$

$$I_{14} = \int_{-\frac{h(r)}{2}}^{\frac{h(r)}{2}} \left[z^2\frac{C_{12}(z)}{r}\right] dz$$

$$I_{15} = \int_{-\frac{h(r)}{2}}^{\frac{h(r)}{2}} \left[z\frac{2\pi}{h_0}e_{31}(z)\right] dz$$

$$I_{16} = \int_{-\frac{h(r)}{2}}^{\frac{h(r)}{2}} \left[\frac{\pi z}{h_0} e_{31}(z)\sin(\frac{\pi z}{h_0})\right] dz$$

$$I_{17} = \int_{-\frac{h(r)}{2}}^{\frac{h(r)}{2}} [z(C_{11}(z) + C_{12}(z))(-\alpha_1(z)T(r))]dz$$

$$I_{18} = \int_{-\frac{h(r)}{2}}^{\frac{h(r)}{2}} [zC_{13}(z)(-\alpha_3(z)T(r))]dz$$

$$I_{21} = \int_{-\frac{h(r)}{2}}^{\frac{h(r)}{2}} [C_{55}(z)]dz$$

$$I_{22} = \int_{-\frac{h(r)}{2}}^{\frac{h(r)}{2}} \left[-e_{15}(z)\cos(\frac{\pi z}{h_0})\right] dz$$